Title

Characterization of vibrational wave packets by core-level high-harmonic transient absorption spectroscopy

Journal

Physical Review A, 88(2)

ISSN

2469-9926

Authors

Hosler, Erik R
Leone, Stephen R

Publication Date

2013-08-01

DOI

10.1103/physreva.88.023420

Peer reviewed

Characterization of vibrational wave packets by core-level high-harmonic transient absorption spectroscopy

Erik R. Hosler and Stephen R. Leone*

Departments of Chemistry and Physics, University of California, Berkeley, California 94720, USA and Chemical Sciences Division, Lawrence Berkeley National Laboratory, Berkeley, California 94720, USA

(Received 22 February 2013; published 23 August 2013)

The ground-state vibrational wave packet produced by strong-field ionization of Br_2 is characterized by femtosecond high-harmonic transient absorption spectroscopy. Vibrational motion is observed in time by a change in the 3*d* core-level transition energy with bond length 0.14 eV/pm to higher energies at shorter bond lengths. The wave packet has the expected period of 104 fs for the predominant v_0v_1 vibrational quantum beat, which is prepared near the outer turning point with a phase of $0.21\pi \pm 0.05\pi$ due to the preferential ionization at short bond lengths. Simultaneous observation of a wave packet on the Br_2^+ $^2\Pi_{g,3/2}$ ground state, prepared at the equilibrium bond distance of the ion, confirms preferential ionization near the inner turning point of the neutral. The Br_2 ground-state wave packet has a degree of coherence ranging between 0.19 and 0.24, where unity is perfect coherence. The results utilize the sensitivity of core-level transient absorption spectroscopy to bond length and charge state, providing a means to analyze the formation and evolution of vibrational wave packets.

DOI: 10.1103/PhysRevA.88.023420 PACS number(s): 33.80.Rv, 33.20.Rm, 42.50.Hz, 82.53.−k

I. INTRODUCTION

The interaction of diatomic molecules with intense near-infrared fields has been extensively researched both theoretically and experimentally to understand various aspects of molecular tunnel ionization [1], dissociative ionization [2], bond softening [3], and wave-packet formation [4]. Of particular interest is the formation of electronic ground-state vibrational-level superpositions, wave packets, due to preferential ionization as a function of internuclear separation. Two general classes of mechanisms have been invoked to explain the phenomena, one in terms of the minimum ionization energy of the unperturbed potentials [5,6], and the other in terms of a critical internuclear separation at which enhanced ionization occurs for the perturbed potentials [7,8]. Unraveling the precise composition and phase of the wave-packet motion can be challenging [9], due to the difficulty in obtaining specific information about the wave-packet localization in the time-resolved probe step. Extreme ultraviolet (XUV) core-level spectroscopic probing can provide a previously unrecognized bond-length-specific detection of vibrational wave packets. Coupled with the element-selective, oxidation- and charge-state-sensitive nature of core-level spectroscopic transitions, ultrafast high-harmonic transient absorption spectroscopy is a powerful means to investigate strong-field ionization dynamics [10–13].

The tunneling rate of molecules is dependent on the ionization energy versus internuclear separation. For diatomic molecules this amounts to a dependence on the bond length (R), the degree to which the laser field perturbs the potential energy curves, and the orientation of the molecular axis with the polarization of the laser electric field [14–16]. Ionization of molecules at R other than the equilibrium bond length, R_0, preferentially depletes the neutral ground-state vibrational states, leaving the remaining ground-state vibrational amplitude near the inner or outer turning point. This nonuniform ionization scheme yields a ground-state vibrational wave packet, and the process is known as the Lochfraß mechanism when applied to the unperturbed potentials [5,6,17].

Lochfraß has been demonstrated for the strong-field ionization of H_2 and D_2 [5,6], where increased ionization on the outer turning point of the molecular ground-state potential is observed to produce a vibrational wave packet. R-dependent ionization of H_2 and D_2 has been explained in terms of both the field-free Born-Oppenheimer and strong-field perturbed potential curves, but in both cases the ionization energy decreases (ionization rate increases) with increasing bond length. In I_2, depending on field strength, strong-field ionization has been shown to lead to preferential ionization at a bond length much larger than expected from the field-free molecular potential curves due to distortion of the potentials by the strong laser field [8]. As the bond stretches, the probability of tunnel ionization at an atomic center increases dramatically and peaks at a critical (elongated) internuclear separation, R_c. This R_c ionization mechanism thereby prepares a ground-state vibrational wave packet at the inner turning point.

In this paper the strong-field ionization dynamics of Br_2 and the resulting ground-state and ion-state vibrational wave packets are explored by a weakly interacting high-order harmonic transient absorption probing of 3*d* core-level transitions in the Br atom. The core-level transition energies exhibit a strong dependence on internuclear separation, which allows a definitive analysis of the phase and composition of the beat frequencies in the vibrational wave packet. The method provides a general means to investigate vibrational wave packets with resolution of the internuclear separation and charge state without distorting the ground-state potential.

Figure 1 schematically outlines the experiment. A minimum 800-nm ionizing field selectively depletes the thermally distributed (300 K) vibrational population of the Br_2 $^1\Sigma_g^+$ ground state at short R, corresponding to the minimum ionization energy of the field-free Born-Oppenheimer potentials. A ground-state vibrational wave packet is prepared at the outer

*Corresponding author: srl@berkeley.edu

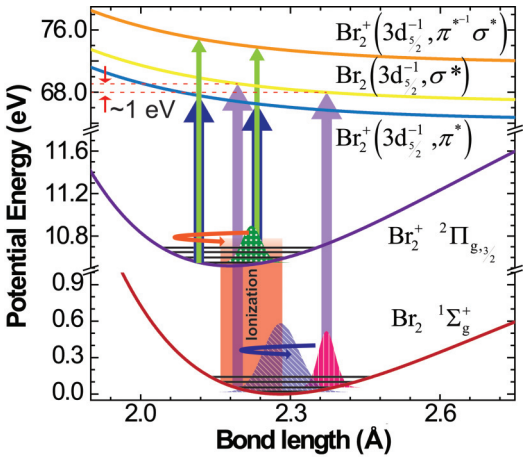

FIG. 1. (Color online) Schematic potential energy diagram of the strong-field ionization of Br_2 showing R-dependent ionization (preferred ionization region shaded in red) and the sensitivity of core-level absorption to the motion of the generated vibrational wave packet on the $^1\Sigma_g^+$ surface. Colored Gaussians illustrate relevant probability densities: (diagonal hatch, blue online) incoherent Br_2 $^1\Sigma_g^+$ Boltzmann population before ionization, (vertical hatch, orange online) exaggerated v_0v_1 vibrational wave packet resulting from strong-field ionization, (polka dot, green online) Br_2^+ $^2\Pi_{3/2,g}$ vibrational wave packet. The Br_2 $^1\Sigma_g^+$ and Br_2^+ $^2\Pi_{3/2,g}$ potentials are taken from literature Morse potential values, and the core-hole excited states are calculated via REW-TD-DFT.

turning point. The time-evolving vibrational wave packets of the neutral and the ion are monitored via absorption of the Br $3d_{5/2,3/2}$ core levels. The transition energy of this absorption is R dependent; it results in up to a 1-eV change between the $^1\Sigma_g^+$ v_1 state inner and outer turning points when probed to the $3d_{5/2,3/2}^{-1}$ core-hole state (nl_j^{-1} symbolizes a hole in the atomic nl orbital with angular momentum j; λ^{-1} is used to symbolize a hole in a molecular orbital $\lambda = \{\sigma,\pi,\ldots\}$).

For this investigation, the peak ionizing laser intensity of 1.6×10^{14} W/cm^2 was chosen to achieve strong-field ionization just at the threshold, resulting in a high contrast change in optical density of the neutral core-level transitions with vibrational motion. Experimental evidence is presented for the formation of a ground-state vibrational wave packet primarily composed of the v_0v_1 vibrational beat in Br_2 and initially prepared at the outer turning point by the strong-field ionization. An estimate is made for the degree of coherence of the Lochfraß ground-state wave packet. The Br_2 ground to core-hole excited state transition energy is measured to be extremely sensitive to internuclear separation, approximately 0.14 eV/pm. The sensitivity of the XUV absorption allows for direct detection of the vibrational wave-packet dynamics and preparation. Previous core-level excitation experiments recognized incoherent vibrational excitation as a broadening of the absorption features [18], while here coherent motion manifests as a distinct shift of the core-level transition energy. This experiment demonstrates the utility of XUV transient absorption as a bond-length-specific probe of vibrational wave-packet dynamics, allowing determination of the superposition's characteristics and preparation even when a small range of bond lengths is explored.

II. CALCULATIONS

The dynamics of the Br_2 $^1\Sigma_g^+$ vibrational wave packet are measured via femtosecond XUV transient absorption to determine its localization and composition. R-dependent Ammosov-Delone-Krainov (ADK) theory is employed to model the strong-field ionization of Br_2. Propagation of the resulting vibrational wave packet, coupled with time-dependent density functional theory (TD-DFT), predicts the R-dependent core-hole transitions and thus models the dynamic XUV absorption signal. The combination of the experimental results and ADK ionization model allows for a straightforward detection and interpretation of the strong-field-generated vibrational wave packet, including determination of its vibrational-level beat composition (v_iv_j) and phase.

Tunnel ionization calculations invoking R-dependent, vibrational-level-specific, ADK theory (R_v-ADK) are performed to predict the Br_2 $^1\Sigma_g^+$ vibrational-level populations after ionization from an initial Boltzmann distribution at 300 K [19]. Literature Morse potential parameters for the Br_2 $^1\Sigma_g^+$ and Br_2^+ $^2\Pi_{g,3/2}$ states are employed in the calculations [20,21]. At 300 K (the conditions of the experiment), the following static square vibrational-level wave function coefficients up to v_3 are taken from the Boltzmann distribution: $|c_0^0|^2 : |c_1^0|^2 : |c_2^0|^2 : |c_3^0|^2 = 79\%{:}17\%{:}3\%{:}{<}1\%$, given the incoherent probability density of the vibrational states is $|c_0^0\psi_{v=0}|^2 + |c_1^0\psi_{v=1}|^2 + \cdots + |c_n^0\psi_{v=n}|^2 = 1$. Integrating the ionization probability with respect to R of each vibrational state over all bond lengths indicates ionization from v_1 is 5% more likely than from v_0, while integration from zero to $R_0^{Br_2}$ indicates ionization from v_1 is 10% more likely than from v_0 over this range. R_v-ADK therefore predicts both increased ionization of higher vibrational states as well as selective ionization at $R < R_0$, indicating the remaining vibrational probability density is partially localized toward the outer turning point.

Tunnel ionization is facilitated by suppression of the electron binding potential by the interacting laser electric field, and while the impact on the nuclear potential curves is similar, perturbation of the Born-Oppenheimer curves at low ionizing field intensities is minimal [6]. Here, we calculate the R_v-ADK tunnel ionization rates according to the ionization energy with R of the field-free Born-Oppenheimer potential curves. This is an accurate approximation within the experimentally chosen ionizing pump field intensity set to achieve threshold ionization of Br_2.

Restricted excitation window TD-DFT (REW-TD-DFT) [22,23] calculations are performed to model the $3d_j^{-1},\sigma^*$ core-hole excitation at all experimentally accessed bond lengths, where $3d_j^{-1},\sigma^*$ is the final-state electronic structure. The calculations do not take into account the spin-orbit state of the core level, but rather determine a spin-orbit averaged result, which is generally applicable to both the $3d_{5/2}^{-1},\sigma^*$ and $3d_{3/2}^{-1},\sigma^*$ states. It is found that the core-hole excited state is highly repulsive around $R_0^{Br_2}$ as shown in Fig. 1 and the resulting transition energies in Fig. 2, which is consistent with the bond order of a system with a $3d$ core hole and an additional electron in a σ^* orbital [24]. At large R's, the XUV transition energy to the core-hole excited states is less than at small R's. Thus the core-level transition energy of a vibrational wave packet oscillates in time. Combining the results of R_v-ADK and

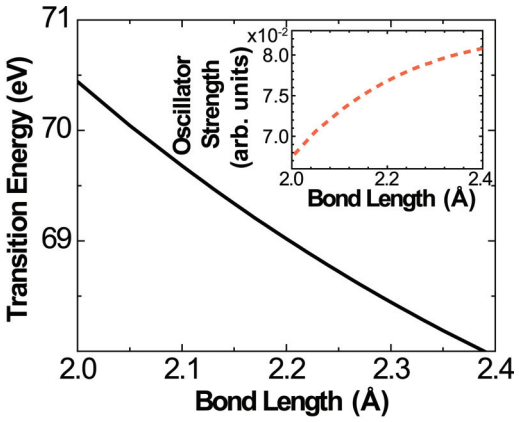

FIG. 2. (Color online) Variation of XUV transition energy with internuclear separation as calculated by REW-TD-DFT calculations employing B3LYP/6-311g* model chemistry. Inset shows the change in the calculated oscillator strength with internuclear separation.

REW-TD-DFT allows for calculation of the XUV absorption at all times and bond lengths, yielding the predicted transient absorption signal shown later.

III. EXPERIMENTAL METHODS

The experimental apparatus is presented in Fig. 3 and has been described in detail previously [25]. The high-harmonic source was changed from a capillary waveguide to a semi-infinite gas cell [26] for increased pulse-to-pulse XUV stability and a 10^3 increase in photon flux. The semi-infinite gas cell is 36 cm long, pressurized with 16.0 kPa of neon, and employs a 0.8-mm-thick Teflon foil to create the XUV exit aperture by laser vaporization. The high-harmonic generation process is driven by 800 nm (1.6 mJ) + 400 nm (25 μJ), 40-fs, 1-kHz linearly polarized light, producing both even- and odd-order harmonics of the fundamental. Removing the inversion symmetry of the driving laser electric field limits XUV pulse generation to once every full optical cycle of the driving laser and generates both the even- and odd-order harmonics [27]. The decrease in XUV pulse production increases the continuum observed between adjacent harmonics resulting from the reduced interference between pulses in the XUV pulse train. The increased spectral coverage of the even and odd harmonics improves the effectiveness of the XUV probe, increasing the signal-to-noise ratio of absorption features between adjacent odd harmonics. The XUV light is focused (beam waist = $w_0 = 20$ μm) into a sample gas cell filled with 3.4 kPa of Br_2 and overlapped at a 1° crossing angle with a 180-μJ, 800-nm pump pulse ($w_0 = 42$ μm) for strong-field ionization; the polarization is parallel to the XUV probe. The XUV transient absorption signal is obtained by measuring the optical density (A) of the transient species relative to the static absorption in the absence of the pump pulse to yield the change in optical density (ΔA). Transient absorption spectra are collected from -0.3 to 40 ps in 20-fs steps averaging 16 scans with an integration time of 0.2 s at each time delay. Each spectrum is referenced to a "pump-off" spectrum utilizing an electronic shutter to block the pump beam, allowing for correction of the fluctuation in XUV flux. The temporal resolution of the instrument is 25 ± 5 fs, as determined by the rise time of the strong-field ionization of $Xe \rightarrow Xe^+$ measured by the $5p_{3/2}^{-1}(^2P_{3/2}) \rightarrow 4d_{5/2}^{-1}(^2D_{5/2})$ transition at 55.4 eV [28,29].

IV. RESULTS AND DISCUSSION

A portion of the transient absorption spectra of the strong-field ionization of Br_2 is presented in Fig. 4. The multifeature resonances oscillating in both optical density

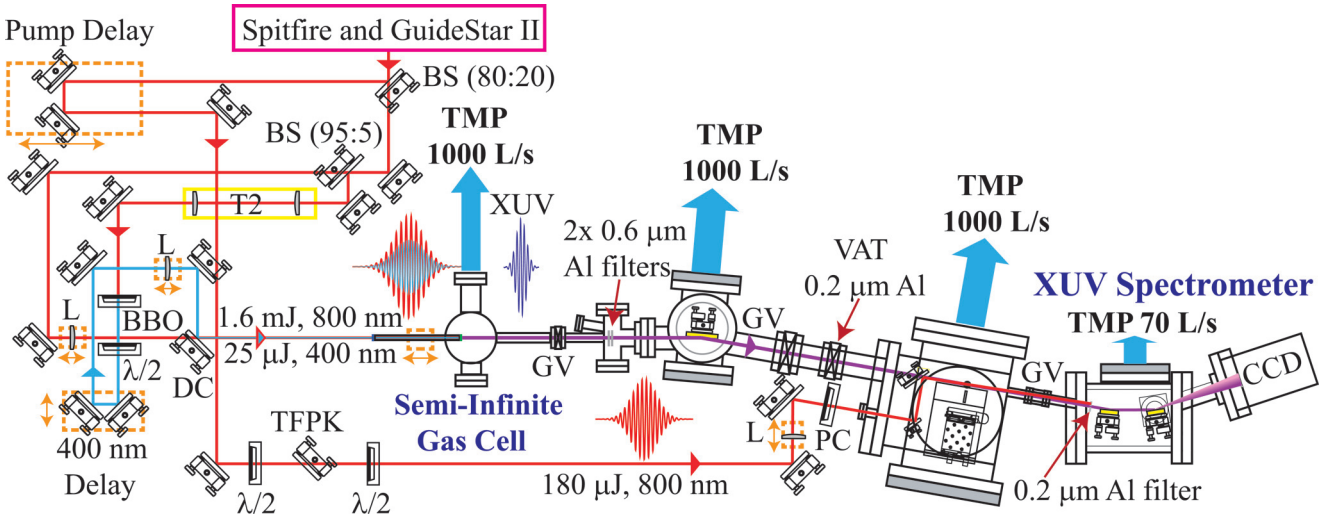

FIG. 3. (Color online) Schematic of the experimental apparatus for 800-nm strong-field pump and XUV probe, utilizing a semi-infinite gas cell for high-harmonic generation of the XUV probe. The pointing of the Spitfire Pro beam has been actively stabilized utilizing a Newport GuideStar II. GV: Gate Valve; VAT: VAT window gate valve with 200-μm Al foil mounted; $\lambda/2$: half-wave plate; T2: 2:1 lens telescope; BS (T:R) Beam splitter with transmission (T) and reflection (R) ratio; DC: Dichroic mirror; L: lens; BBO: Type 1 beta-barium-borate crystal for second-harmonic generation; TFPK: low-dispersion thin-film polarizer; PC: Polarcor linear polarizer; CCD: PIXIS:XO 100B x-ray camera; TMP: Turbomolecular pump. Dashed line boxes (orange online) and arrows indicate a translational stage. The high-harmonic driver and pump beam are focused by 78-cm and 45-cm focal length lenses, respectively.

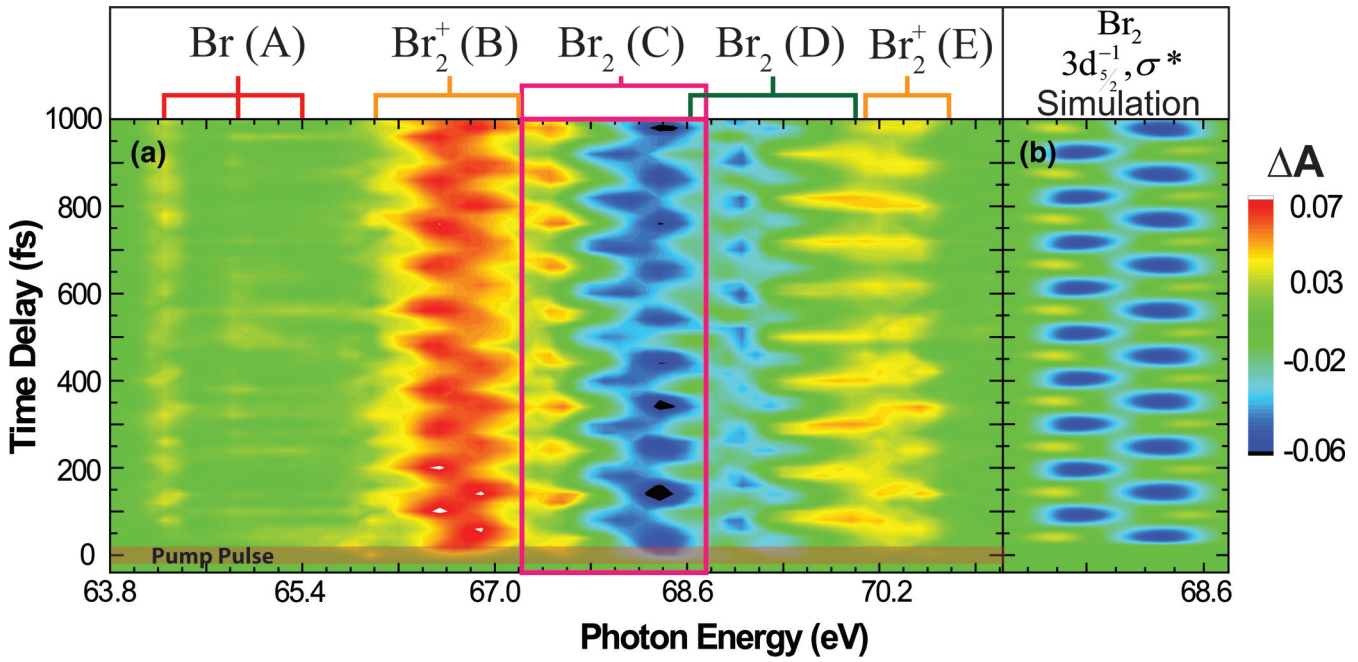

FIG. 4. (Color) Comparison of experimental data and simulation of the core-level transient absorption signal of strong-field ionized Br_2. (a) False color map of the experimental absorption signal in time using an ionizing 800-nm pump field of 1.6×10^{14} W/cm^2 (shown at $t = 0$ in transparent red). The $^1\Sigma_g^+$ ground-state wave packet is observed to be launched on the outer turning point of the potential with a period of 104 fs by transitions (C) and (D), corresponding to the Br_2 $^1\Sigma_g^+$ $\sigma^{*-1} \rightarrow 3d_{5/2}^{-1}$ and $\sigma^{*-1} \rightarrow 3d_{3/2}^{-1}$ transitions, respectively. The $^2\Pi_{g,3/2}$ ion ground-state vibrational wave packet is observed through transitions (B, $\pi^{*-1} \rightarrow 3d_{5/2}^{-1}$) and (E, $\sigma^{*-1} \rightarrow 3d_{5/2}^{-1}$), with a 94-fs period. Atomic Br transitions are labeled (A), corresponding to the $^2P_{3/2} \rightarrow {}^2D_{5/2}$ (64.4 eV), $^2P_{1/2} \rightarrow {}^2D_{3/2}$ (65.1 eV), and $^2P_{3/2} \rightarrow {}^2D_{3/2}$ (65.4 eV) transitions. (b) Simulation of the core-level absorption of the $^1\Sigma_g^+$ wave packet probed to the $3d_j^{-1}$ core-hole state [cf. experimental data (C) boxed in pink] employing R_v-ADK theory and REW-TD-DFT calculations for the strong-field ionization response and core-hole excitation, respectively.

and transition energy centered at 68.3 eV ($^1\Sigma_g^+,\sigma^{*-1} \rightarrow 3d_{5/2}^{-1}$) and 69.4 eV ($^1\Sigma_g^+,\sigma^{*-1} \rightarrow 3d_{3/2}^{-1}$) correspond to neutral molecular core-hole excitations, recovered by measuring the ΔA relative to the static absorption in absence of the pump pulse. The $^1\Sigma_g^+$ Br_2 transitions predominantly appear as negative changes in optical density as the $^1\Sigma_g^+$ population is depleted by the ionizing 800-nm field. The evolving $^1\Sigma_g^+$ vibrational wave packet presents positive and negative features away from $R_0^{Br_2}$ as shown in both Figs. 4 and 5. The oscillating transitions centered at 66.8 eV ($^2\Pi_{g,3/2},\pi^{*-1} \rightarrow 3d_{5/2}^{-1}$) and 70.4 eV ($^2\Pi_{g,3/2},\sigma^{*-1} \rightarrow 3d_{5/2}^{-1}$) probe the Br_2^+ ion $^2\Pi_{g,3/2}$ ground-state vibrational wave packet to the ion core-hole excited states. The core-hole final state of the ion results from filling either the strong-field-generated π^{*-1} hole or the unoccupied σ^{*-1} state with the promoted $3d$ electron. Additionally, a narrow absorption feature with a 0.2-eV Gaussian full width at half maximum (FWHM) is observed at 66.6 eV overlapping with the molecular ion resonance and assigned to the Br^+ $^2P_3 \rightarrow {}^3D_3$ and $^1D_2 \rightarrow {}^1F_2$ transitions. The Br^+ assigned feature is too narrow to be a molecular transition and is constant in time with respect to energy and amplitude, indicating it does not stem from the vibrational wave-packet dynamics. Current work at the Advanced Light Source has shown that both assigned atomic transitions have similar absolute photoabsorption cross sections around the observed energy with a FWHM less than the instrumental resolution [30].

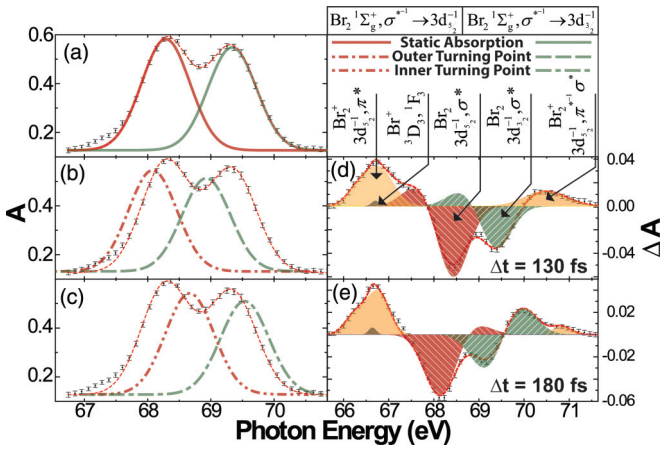

FIG. 5. (Color online) Core-level $3d_{5/2,3/2}$ absorption spectra of Br_2 (black dots with standard error of the mean). (a) The static absorption "pump-off" signal of Br_2 fit to two Gaussians, each of 0.8 eV width, resulting in the dotted trace (red online). (b) Outer turning point and (c) inner turning point correspond to the time-evolving absorption of the $^1\Sigma_g^+$ simulated vibrational wave-packet signal at the turning points of the potential relative to the static absorption signal. (d) The observed transient absorption signal at 130-fs pump-probe delay (outer turning point), and (e) the transient absorption signal at 180-fs delay (inner turning point). The transitions are labeled according to the electronic structure of the final state.

Examining Fig. 4, it is clear from the spectral oscillation that the vibrational amplitude in the Br_2 $^1\Sigma_g^+$ state becomes at least partially coherent from the population transfer by the strong-field depletion. Fast-Fourier transform (FFT) of the data versus time yields ~ 1 cm^{-1} spectral resolution as shown in Fig. 6. The three natural isotopic Br_2 v_0v_1 vibrational beats are observed with a ratio of $1{:}[1.8 \pm 0.2]{:}1$ ($^{79-79}Br_2$: $^{79-81}Br_2$: $^{81-81}Br_2$), where the natural abundance is 1:2:1. Accounting for the isotopes of Br_2, it is clear the dominant vibrational beat of the $^1\Sigma_g^+$ wave packet is v_0v_1, with little to no higher-level contributions. The $^{79-81}Br_2$ v_0v_1 beat is expected to have a frequency of 321 cm^{-1}, or a period ($\tau_{v_0v_1}$) of 104 fs [20]. Fitting the transient absorption signal at 68.3 eV with a convolution of Heaviside (strong-field depletion), Gaussian (instrumental temporal resolution), and cosinusoidal (coherence) functions yields an oscillatory period of 104 ± 1 fs, an amplitude of 0.008 ± 0.001 A, and a phase of $0.21\pi \pm 0.05\pi$ measured relative to the center of the strong-field depletion response of Br_2, as shown in the inset of Fig. 6. Correlating the phase measurement with the REW-TD-DFT calculation indicates that the generated vibrational wave packet is launched at the outer turning point (lower XUV transition energy) [7].

The effectiveness of tunnel ionization to prepare a v_0v_1 ground-state vibrational wave packet is gauged by the degree of coherence, measured by the magnitude of the off-diagonal terms of the density matrix $\rho_{v_0v_1}$. The probability of finding a molecule in vibrational states $\{v_0, \ldots, v_n\}$ after the pump pulse, with $\chi_j = c_j \psi_{v=j} e^{-i\omega_j t}$, is given for just two states by

$$\rho_{v_0v_1} = \begin{Bmatrix} |c_0^2| & c_1^* c_0 g_{v_0v_1} \cos\left[\omega_{v_0v_1} t + \varphi_{v_0v_1}\right] \\ c_0^* c_1 g_{v_0v_1} \cos\left[\omega_{v_0v_1} t + \varphi_{v_0v_1}\right] & |c_1^2| \end{Bmatrix}, \tag{1}$$

where $\omega_{v_0v_1}$, $\varphi_{v_0v_1}$, and $g_{v_0v_1}$ are the frequency, phase, and degree of coherence of the v_0v_1 vibrational beat, respectively. The diagonal elements of $\rho_{v_0v_1}$ account for the neutral depletion ΔA, and the off-diagonal elements describe the oscillation in the ΔA amplitude due to wave-packet motion. Comparing the Br_2 transient depletion optical density at positive time delays and the $3d_{5/2} \rightarrow \sigma^*_{\mathrm{LUMO}}$ static absorption, $\sim 5\%$ of the Br_2 population in the XUV focal volume is determined to be ionized by the pump, i.e., $\mathrm{Tr}[\rho_{v_0v_n}] = 0.95$.

Higher vibrational levels beyond v_1 may be involved in the ground-state wave packet, which would lead to multiple $g_{v_iv_j}$ terms. The FFT in Fig. 6 shows that v_0v_1 is the dominant quantum beat, and coherence terms involving v_2 and greater are found to be beyond the detection limit of the instrument. For determining the ground-state vibrational wave-packet degree of coherence, contributions of v_2 and greater are neglected, but a static population in v_2 is retained to account for the $\mathrm{Tr}[\rho_{v_0v_n}]$. Furthermore, convolution of the instrument response function with the v_0v_2 overtone frequency indicates the beat is beyond the temporal resolution of the instrument and therefore may be discounted in the determination of the wave packet's degree of coherence.

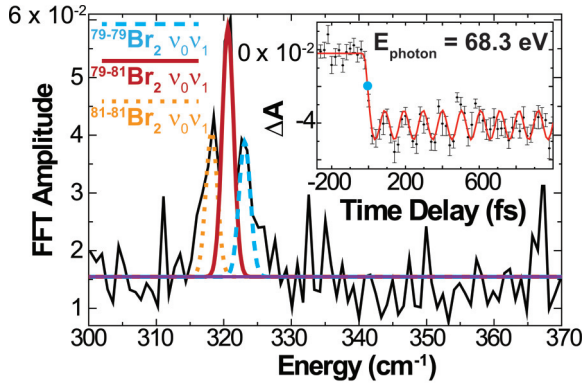

FIG. 6. (Color online) Fast-Fourier transform of the transient absorption signal from 67.4 to 70.5 eV. The inset shows the fit of the Br_2 $^1\Sigma_g^+$, $\sigma^{*-1} \rightarrow 3d_{5/2}^{-1}$ transient absorption signal at 68.3 eV. The wave packet is measured to have a 104 ± 1-fs period, an oscillatory amplitude of 0.008 ± 0.001 ΔA, and a phase of $0.21\pi \pm 0.05\pi$ relative to the Br_2 strong-field response (blue dot, -5 ± 2 fs). Error bars correspond to one standard error of the mean.

The density matrix $\rho_{v_0v_1}$ is utilized to determine the degree of coherence, which is evaluated at the center of the Gaussian fit of the $^1\Sigma_g^+, \sigma^{*-1} \rightarrow 3d_{5/2}^{-1}$ static absorption. Introduction of $g_{v_0v_1}$ into the density matrix formalism provides a means to put limits on the degree of coherence of the vibrational beat. Here, a $g_{v_0v_1}$ of unity indicates perfect coherence, while zero specifies a random phase between the two vibrational levels. The change in optical density with pump-probe time delay is then

$$\Delta A(E) = [A_{\mathrm{incoherent}}(E) + A_{\mathrm{coherent}}(E,t)] - A_{\mathrm{static}}(E), \tag{2}$$

$$\left[|c_0^0|^2 |\psi_{v=0}(E)|^2 + |c_1^0|^2 |\psi_{v=1}(E)|^2 + |c_2^0|^2 |\psi_{v=2}(E)|^2\right] p_{\mathrm{XUV}} = A_{\mathrm{static}}(E), \tag{3}$$

$$[|c_0|^2 |\psi_{v=0}(E)|^2 + |c_1|^2 |\psi_{v=1}(E)|^2 + |c_2|^2 |\psi_{v=2}(E)|^2] p_{\mathrm{XUV}} = A_{\mathrm{incoherent}}(E), \tag{4}$$

$$2 * \mathrm{Re}\left\{c_0^* c_1 g_{v_0v_1} \psi^*_{v=0}(E) \psi_{v=1}(E) \cos\left[\omega_{v_0v_1} t + \varphi_{v_0v_1}\right]\right\} p_{\mathrm{XUV}} = A_{\mathrm{coherent}}(E,t), \tag{5}$$

where $A_{\mathrm{incoherent}}(E)$ and $A_{\mathrm{coherent}}(E,t)$ relate to the absorption amplitude of the incoherent and coherent populations, respectively. $A_{\mathrm{coherent}}(E,t)$ is given by the time-dependent amplitude associated with $\cos[\omega_{v_0v_1} t + \varphi_{v_0v_1}]$, and p_{XUV} is an experimentally estimated $^1\Sigma_g^+, \sigma^{*-1} \rightarrow 3d_{5/2}^{-1}$ core-hole absorption probability. The absorption probability is obtained by fitting the static optical density to the incoherent vibrational amplitude multiplied by a constant relating to the experimental conditions (transition strength, gas density, interaction length)

at 68.3 eV. An estimate for $g_{v_0v_1}$ can then be determined by considering the extreme case where 5% of the initial $^1\Sigma_g^+$ population is removed entirely from only one vibrational level. The range of $g_{v_0v_1}$ satisfying the experimental data as interpreted by Eqs. (3)–(5) is $0.19 \rightarrow 0.24$.

A previous experiment also demonstrated a lack of perfect coherence resulting from strong-field ionization, which was attributed to scrambled vibrational-level phases [7]. Ionization of the ground state occurs over the entirety of the pump pulse, constantly varying the value of $\varphi_{v_0v_1}$ in the generated wave packet. Therefore, phase scrambling is dependent on the ratio of the experimental pump pulse duration to the vibrational beat time, which are similar ($\tau_{\text{pump}} \approx \tau_{v_0v_1}/2$). Employing pump and probe pulses on the order of 10 fs each, the degree of coherence may be larger and it would also be possible to observe the vibrational overtone, definitively establishing the vibrational state distribution of the wave packet.

We can also consider the impact of a possible incoherent v_2 population on the degree of coherence. If population is transferred incoherently by Raman excitation to higher vibrational states, this would reduce the population percentage in v_0 and v_1. Recalculating $g_{v_0v_1}$ with a 50% increase in the incoherent v_2 population from v_0 or v_1 still yields a $g_{v_0v_1}$ significantly less than 1, indicating that the impact of neglecting incoherent Raman excitations at this field intensity is minor.

The agreement between the REW-TD-DFT calculations and experiment definitively establishes the initial localization of the v_0v_1 wave packet on the outer turning point of the $^1\Sigma_g^+$ potential for Br_2 (i.e., depletion occurs on the inner turning point). Several mechanisms are considered to impact ground-state vibrational wave packets including impulsive stimulated Raman scattering [31], R_c ionization [7,8], and Lochfraß [5]. At the low laser field applied here, impulsive stimulated Raman scattering does not directly account for the ionization mechanism and the correlation between the Br_2 $^1\Sigma_g^+$ and Br_2^+ $^2\Pi_{g,3/2}$ vibrational wave packets. Raman pumping would also generate wave packets involving higher vibrational states due to population redistribution, a topic of a future publication including intensity dependence and dynamics of the Br_2^+ $^2\Pi_{g,3/2}$ state. R_c ionization predicts depletion of the ground-state probability density at $R > R_0$ caused by field perturbation of the electronic potential and resulting in preparation of the wave packet on the inner turning point. In this work, in contrast to previous studies [8], field dressing of the potentials is not required to rationalize the experimental results, having explicitly worked within the regime of the adiabatic approximation for the strong-field ionization. Lochfraß describes strong-field ionization as occurring predominately at the minimum ionization energy, and no additional mechanism beyond R_v-ADK is required to explain the experimental results here. Selective ionization of vibrational states in Br_2 $^1\Sigma_g^+$ to generate a vibrational wave packet initially localized near the outer turning point is indicative of the strong dependence of the ionization energy on R and v for the unperturbed potentials.

The change in the $3d_{5/2}^{-1}$ core-hole transition energy with bond length may be estimated knowing the beat composition of the Br_2 $^1\Sigma_g^+$ wave packet and the transition energy at the molecular potential inner and outer turning point. The maximum shift in transition energy is experimentally found to be 0.5 eV from the static resonance. Representing the $^1\Sigma_g^+$ state by the spectroscopically determined Morse potential [20], the change in R is 7 pm from the inner to outer turning points of a v_0v_1 wave packet, calculated relative to the mean of the vibrational amplitude. The $^1\Sigma_g^+, \sigma^{*-1} \rightarrow 3d_{5/2}^{-1}$ change in transition energy with bond length is thereby determined to be approximately 0.14 eV/pm, indicating the $3d_{5/2}^{-1}$, σ^* state is repulsive around $R_0^{Br_2}$. Therefore, a high degree of sensitivity for the XUV absorption energy with bond length is realized, facilitating direct probing of a vibrational wave packet exploring even a small oscillatory range.

Considering the ion, evolution of the internuclear separation of the ion leads to a similar change in the XUV transition energy to the corresponding core-hole excited states as observed with the neutral wave packet as seen in Figs. 4 and 5. The lack of a static reference feature for the ion means that the transient absorption signal is always positive and is dependent only on the transition energy and oscillator strength with R. The line shape of the resonance at each time delay is a direct measure of the vibrational wave-packet amplitude. Examining the ion vibrational wave packet at the molecular potential turning points shows the vibrational amplitude piling up, spectrally manifesting as an increase in optical density and a narrowing of the line shape as seen in Fig. 4. Although this result could be expected from similar investigations in the visible regime, it illustrates the effectiveness of bond-length-specific XUV probing for directly visualizing vibrational dynamics.

Intuitively, Franck-Condon ionization of $Br_2(^1\Sigma_g^+) \rightarrow Br_2^+(^2\Pi_{g,3/2})$, such as with a single photon, predicts the ion vibrational wave packet to be initially localized at $R_0^{Br_2}$ [32], toward the $^2\Pi_{g,3/2}$ outer turning point (lower XUV transition energy) as $R_0^{Br_2^+} < R_0^{Br_2}$, exciting a broad manifold of vibrational states centered on v_2. Contrariwise, Lochfraß predicts preferential depletion of the $^1\Sigma_g^+$ vibrational population at the inner turning point, preparing the Br_2^+ $^2\Pi_{g,3/2}$ wave packet close to $R_0^{Br_2^+}$. Examining the Br_2^+ $3d_{5/2}^{-1}$, π^* transition energy in Fig. 4 at ~20-fs pump-probe delay shows the ion superposition is birthed at $R \approx R_0^{Br_2^+}$, indicative of Lochfraß. Fitting the measured ion vibration signal at 66.7 eV in the same manner as the neutral reveals the vibrational period is 93 ± 1 fs ($\tau_{v_0v_1}^{Br_2^+} = 92$ fs) [21] and the phase is similar to the neutral wave packet. FFT of the ion wave packet reveals only a broad feature centered at 360 cm^{-1}. Although the exact composition of the vibrational wave packet cannot be retrieved, it can be inferred by the width of the FFT feature that several vibrational levels are substantially populated. Comparable results are observed for the strong-field ionization of H_2, where v_0 to v_2 are populated almost equally [33].

V. CONCLUSIONS AND FUTURE OUTLOOK

Femtosecond core-level XUV transient absorption spectroscopy is a method with unprecedented chemical and temporal capabilities [25,28,29,34]. The present work shows XUV core-level transient absorption spectroscopy to be an effective method for probing internuclear separation and determining the real-time frequency, phase, composition, and

position of vibrational wave packets. The initial localization of the strong-field-generated wave packet on the Br_2 $^1\Sigma_g^+$ state is definitively established on the outer turning point of the potential, substantiated via R_v-ADK plus REW-TD-DFT calculations. At this field intensity, there is no indication of substantial vibrational population redistribution to higher levels as a result of Raman pumping or enhanced ionization due to an R_c-ionization mechanism, as confirmed by the FFT of the $^1\Sigma_g^+$ wave packet and its initial localization.

Finally, we emphasize the far-reaching consequences of bond-length-sensitive XUV transient absorption: Here, we have demonstrated core-level, bond-length-specific probing on the femtosecond time scale for a homonuclear diatomic. The natural extension is to investigate heteronuclear and polyatomic systems, fully utilizing the element-specific capabilities of the XUV probe and allowing detection of vibrational motion with bond-length specificity at multiple reporter atoms. Though the current experiment utilized Lochfraß to launch the vibrational motion, it is not crucial to the success of the x-ray transient absorption method to reveal vibrational wave-packet information. Expansion of this technique to the attosecond regime may facilitate detection of correlated electronic and nuclear wave packets in real time. This has implications for studying phenomena such as charge transfer or localization and non-Born-Oppenheimer dynamics with unprecedented resolution and clarity [35,36].

ACKNOWLEDGMENTS

We thank Scott G. Sayres for numerous fruitful discussions, and Andrew R. Attar and Josh Vura-Weis for experimental contributions. We also thank James S. Prell for the careful reading of this manuscript. This work was supported by the NSF ERC of EUV Science and Technology (Grant No. EEC-0310717) with funding for materials and equipment provided through the Department of Energy Grant No. DE-AC02-05-CH11231 via the LBNL Chemical Sciences Division. S.R.L. acknowledges support of the DoD NSSEFF.

[1] S. Augst, D. Strickland, D. D. Meyerhofer, S. L. Chin, and J. H. Eberly, Phys. Rev. Lett. **63**, 2212 (1989).
[2] K. Codling and L. J. Frasinski, J. Phys. B **26**, 783 (1993).
[3] J. H. Posthumus, J. Plumridge, P. F. Taday, J. H. Sanderson, A. J. Langley, K. Codling, and W. A. Bryan, J. Phys. B **32**, L93 (1999).
[4] L. Fang and G. N. Gibson, Phys. Rev. A **75**, 063410 (2007).
[5] E. Goll, G. Wunner, and A. Saenz, Phys. Rev. Lett. **97**, 103003 (2006).
[6] T. Ergler, B. Feuerstein, A. Rudenko, K. Zrost, C. D. Schroter, R. Moshammer, and J. Ullrich, Phys. Rev. Lett. **97**, 103004 (2006).
[7] L. Fang and G. N. Gibson, Phys. Rev. Lett. **100**, 103003 (2008).
[8] T. Seideman, M. Y. Ivanov, and P. B. Corkum, Phys. Rev. Lett. **75**, 2819 (1995).
[9] L. Fang and G. N. Gibson, Phys. Rev. A **78**, 051402 (2008).
[10] Z.-H. Loh and S. R. Leone, J. Phys. Chem. Lett. **4**, 292 (2012).
[11] M. Holler, F. Schapper, L. Gallmann, and U. Keller, Phys. Rev. Lett. **106**, 123601 (2011).
[12] C. Ott, A. Kaldun, P. Raith, K. Meyer, M. Laux, Y. Zhang, S. Hagstotz, T. Ding, R. Heck, and T. Pfeifer, arXiv:1205.0519v1.
[13] H. Wang, M. Chini, S. Chen, C.-H. Zhang, F. He, Y. Cheng, Y. Wu, U. Thumm, and Z. Chang, Phys. Rev. Lett. **105**, 143002 (2010).
[14] A. Saenz, Phys. Rev. A **66**, 063408 (2002).
[15] A. Saenz, Phys. Rev. A **66**, 063407 (2002).
[16] B. Friedrich and D. Herschbach, Phys. Rev. Lett. **74**, 4623 (1995).
[17] A. Rudenko, T. Ergler, B. Feuerstein, K. Zrost, C. D. Schroter, R. Moshammer, and J. Ullrich, Chem. Phys. **329**, 193 (2006).
[18] C. P. Schwartz, J. S. Uejio, R. J. Saykally, and D. Prendergast, J. Chem. Phys. **130**, 184109 (2009).
[19] J. P. Brichta, W. K. Liu, A. A. Zaidi, A. Trottier, and J. H. Sanderson, J. Phys. B **39**, 3769 (2006).
[20] J. A. Horsley and R. F. Barrow, Trans. Faraday Soc. **63**, 32 (1967).
[21] T. Harris, J. H. D. Eland, and R. P. Tuckett, J. Mol. Spectrosc. **98**, 269 (1983).
[22] K. Lopata, B. E. Van Kuiken, M. Khalil, and N. Govind, J. Chem. Theory Comput. **8**, 3284 (2012).
[23] M. Valiev, E. J. Bylaska, N. Govind, K. Kowalski, T. P. Straatsma, H. J. J. Van Dam, D. Wang, J. Nieplocha, E. Apra, T. L. Windus, and W. de Jong, Comput. Phys. Commun. **181**, 1477 (2010).
[24] O. Takahashi, K. Matsuyama, K. Tabayashi, and K. Yamasaki, J. Phys. B **42**, 245102 (2009).
[25] Z. H. Loh, M. Khalil, R. E. Correa, and S. R. Leone, Rev. Sci. Instrum. **79**, 073101 (2008).
[26] J. Sutherland, E. Christensen, N. Powers, S. Rhynard, J. Painter, and J. Peatross, Opt. Express **12**, 4430 (2004).
[27] X. He, J. M. Dahlström, R. Rakowski, C. M. Heyl, A. Persson, J. Mauritsson, and A. L'Huillier, Phys. Rev. A **82**, 033410 (2010).
[28] Z. H. Loh, M. Khalil, R. E. Correa, R. Santra, C. Buth, and S. R. Leone, Phys. Rev. Lett. **98**, 143601 (2007).
[29] Z.-H. Loh and S. R. Leone, J. Chem. Phys. **128**, 204302 (2008).
[30] A. Aguillar (private communication).
[31] L. Dhar, J. A. Rogers, and K. A. Nelson, Chem. Rev. **94**, 157 (1994).
[32] D. P. Stevenson, J. Am. Chem. Soc. **82**, 5961 (1960).
[33] X. Urbain, B. Fabre, E. M. Staicu-Casagrande, N. de Ruette, V. M. Andrianarijaona, J. Jureta, J. H. Posthumus, A. Saenz, E. Baldit, and C. Cornaggia, Phys. Rev. Lett. **92**, 163004 (2004).
[34] E. Goulielmakis, Z.-H. Loh, A. Wirth, R. Santra, N. Rohringer, V. S. Yakovlev, S. Zherebtsov, T. Pfeifer, A. M. Azzeer, M. F. Kling, S. R. Leone, and F. Krausz, Nature **466**, 739 (2010).
[35] A. W. Jasper, S. Nangia, C. Zhu, and D. G. Truhlar, Acc. Chem. Res. **39**, 101 (2005).
[36] G. Sansone *et al.*, Nature **465**, 763 (2010).